ISIJ International, Vol. 30 (1990), No. 8, pp. 680-686

Phase Equilibria in Fe–Mn–Al–C Alloys

Kiyohito ISHIDA, Hiroshi OHTANI, Naoya SATOH, Ryosuke KAINUMA and Taiji NISHIZAWA

Department of Materials Science, Faculty of Engineering, Tohoku University, Aramaki Aza Aoba, Aoba-ku, Sendai, Miyagi-ken, 980 Japan.

(Received on December 22, 1989; accepted in the final form on February 16, 1990)

Phase constitutions of Fe–(20–30) wt% Mn–(0–10) wt% Al–C alloys have been investigated by electron probe microanalysis and transmission electron microscopy. The phase relations between austenite and perovskite carbide, $(Fe, Mn)_3AlC$ in the temperature range of 900–1 200°C have been carefully examined. An $L1_2$-type ordered structure, which was reported to be formed in rapidly solidified alloys as a metastable phase has not been detected in specimens aged at temperatures above 600°C.

KEY WORDS: phase diagram; Fe–Mn–Al–C system; perovskite carbide; modulated structure.

1. Introduction

There is currently great interest in studying properties of the Fe–Mn–Al–C alloys with the aim of practical applications to an austenitic stainless steel without Ni and Cr,[1,2] cryogenic materials[3–6] and magnetic alloys.[7] Furthermore, it has been reported that high strength materials were obtained by rapid solidification of the Fe–Al–C base alloys, and that this high strength was mainly due to the formation of γ' phase with $L1_2$ structure.[8,9] However, there have been conflicting results on the existence of the γ' phase not only in rapidly quenched specimens but also in bulk specimens. The formation of the γ' phase has been affirmed by experiments on Fe–Al–C[10–12], Fe–Ni–Al–C[8,9,13] and Fe–Mn–Al–C[8,9,14] alloys, while such occurrence was denied by works on Fe–Al–C[15,16], Fe–Ni–Al–C[17,18] and Fe–Mn–Al–C[19–21] alloys. It is probable that the similarity of electron diffraction patterns from both the perovskite carbide (Fe_3AlC; κ) and the γ' phase caused such confusion. In the present work, the phase equilibria among γ, γ' and κ phases in Fe–(20–30)wt%Mn–(0–10)wt%Al–C alloys between 900 and 1 200°C were studied by means of electron probe microanalysis and TEM observation with a view to contributing to the development of a promising material.

2. Experimental Procedure

Fe–20wt%Mn–Al–C and Fe–30wt%Mn–Al–C alloys were made of electrolytic iron (99.95 %), electrolytic manganese (99.99 %), pure aluminium (99.99 %) and graphite by induction melting under an argon atmosphere. They were cut into small pieces and equilibrated at fixed temperatures between 900 and 1 200°C for 14–210 h.

After examining the microstructure by optical microscope, the composition of each phase in the two-phase specimens was determined by electron probe microanalyzer (EPMA) using a LiF, an ADP and a Pb stearate crystal for Mn Kα, Al Kα and C Kα radiations, respectively. The accelerating voltage for the electron beam and the sample current were kept at 20 kV and 50 nA, respectively. The take-off angle of the spectrometer was 52.5°. The relative intensities were converted to weight fractions, taking corrections on the atomic number, absorption and fluorescence effects into account.

Transmission electron microscopy was performed at 200 kV, where the thin foil specimens were prepared by electropolishing in a mixture of 200 g chromic acid and 200 g phosphoric acid after annealing at 600–1 100°C.

3. Results and Discussion

3.1. Phase Equilibria

The microstructures of specimens annealed between 900 and 1 200°C were observed by optical microscope. Fig. 1 is a typical structure of Fe–30Mn–12Al–1.9C alloy annealed at 1 000°C for 98 h, showing the Widmanstätten pattern of austenite (γ) and perovskite carbide (κ), which have been reported to be stable

Fig. 1. Optical micrograph for Fe–30Mn–12Al–1.9C alloy annealed at 1 000°C, showing parallel lamellae of γ and κ.

phases at higher temperatures.[21] The equilibrium compositions of each phase in Fe–20Mn–Al–C and Fe–30Mn–Al–C alloys are given in Tables 1 and 2, respectively. In these tables, ferrite, austenite, cementite and carbide with the perovskite structure are designated as α, γ, M_3C and κ, respectively. It can be seen that the κ phase appears in alloys with high levels of Al and C and that the equilibrium compositions of Mn in the γ and κ phases are not so different from each other. Therefore, the phase constitutions of Fe–20Mn–Al–C and Fe–30Mn–Al–C alloys are given in two-dimensional figures as Figs. 2 and 3, assuming that the concentrations of Mn in the γ and κ phases are equal. The stable γ region in the Fe–30Mn–Al–C alloy is wider than that in the Fe–20Mn–Al–C alloy. The vertical section diagrams for 9 % Al, which is an aluminium content recommended for high corrosion resistance alloy, are shown in Fig. 4, where the solubility of C in γ decreases rapidly with decreasing temperature and is in good agreement with the results by Choo and Han.[21] It should be noted that it is desirable that the carbon content is less than 1 wt% in Fe–30Mn base alloys to avoid the precipitation of ferromagnetic κ phase, obtaining non-magnetic austenitic alloy. Fig. 5 shows the vertical section at

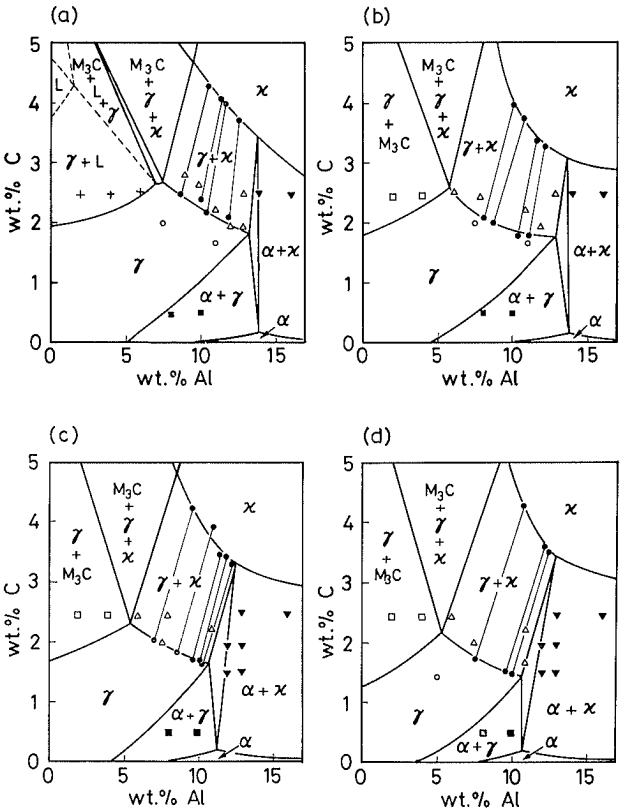

○ γ △ $\gamma+\kappa$ ■ $\alpha+\gamma$ ▼ $\alpha+\kappa$ □ $\gamma+M_3C+\gamma+L$
(a) 1 200°C (b) 1 100°C
(c) 1 000°C (d) 900°C

Fig. 2. Isothermal section diagrams for Fe–20Mn–Al–C alloys.

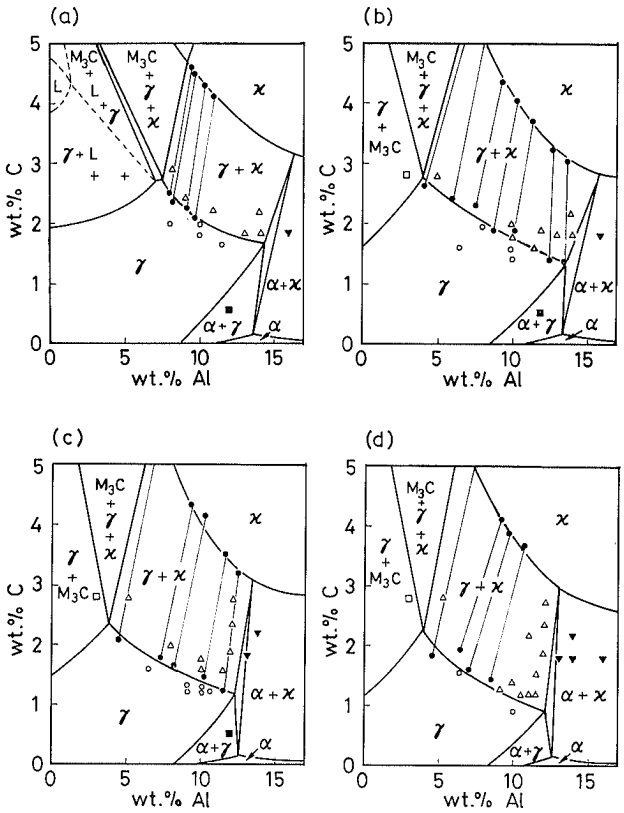

○ γ △ $\gamma+\kappa$ ■ $\alpha+\gamma$ ▼ $\alpha+\kappa$ □ $\gamma+M_3C+\gamma+L$
(a) 1 200°C (b) 1 100°C
(c) 1 000°C (d) 900°C

Fig. 3. Isothermal section diagrams for Fe–30Mn–Al–C alloys.

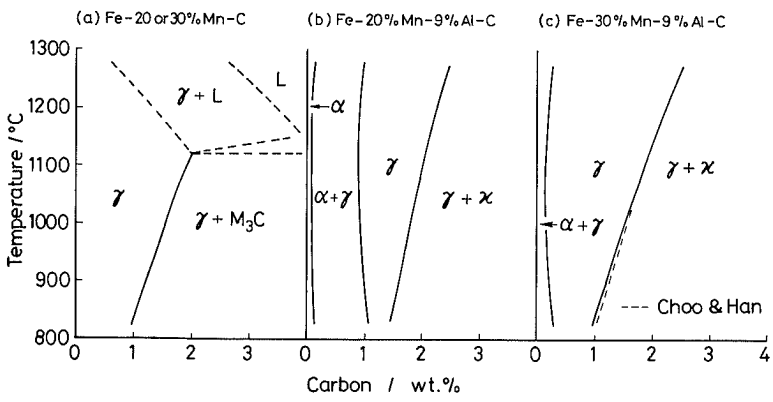

Fig. 4. Vertical section diagrams for Fe–(20–30)Mn–9Al–C alloys.

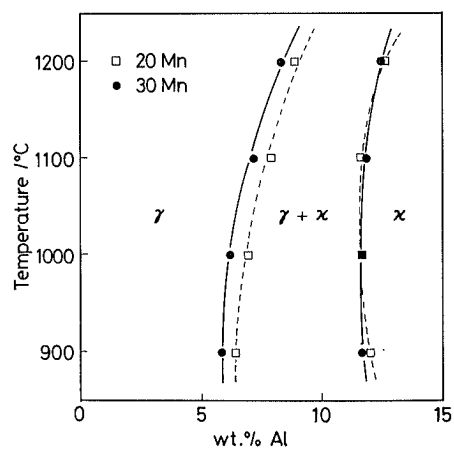

Fig. 5. Vertical section diagram for Fe–(20–30)Mn–Al–C alloy at Al/C= 3.5/1.

Table 1. Equilibrium composition of phases in Fe-20%Mn-Al-C alloys.

Composition of specimen (wt%)		Temp. (°C)	Compositions (wt%)																
			$\gamma/\gamma+\kappa$			$\kappa/\gamma+\kappa$			$\alpha/\alpha+\kappa$			$\kappa/\alpha+\kappa$			$\gamma/\gamma+M_3C$			$M_3C/\gamma+M_3C$		
Al	C		Mn	Al	C	Mn	Al	C	Mn	Al	C	Mn	Al	C	Mn	Al	C	Mn	Al	C
2	2.5	1 100		—			—			—			—		19.2	2.1	2.5	27.6	0.1	6.0
		1 000		—			—			—			—		18.0	2.2	2.0	29.4	0.1	6.2
		900		—			—			—			—		16.8	2.5	1.8	30.4	0.1	6.6
6	2.5	1 100	19.5	5.6	2.5	22.4	8.2	4.6		—			—			—			—	
		1 000	19.4	5.4	2.5	23.0	8.5	4.7		—			—			—			—	
7.5	2.0	1 000	20.0	7.1	2.1	22.9	9.7	4.2		—			—			—			—	
9	2.8	1 200	19.7	8.8	2.5	21.6	10.7	4.3		—			—			—			—	
		1 100	19.5	8.2	2.1	21.3	10.2	4.0		—			—			—			—	
		900	19.2	7.5	1.7	23.3	10.8	4.4		—			—			—			—	
10	2.7	1 100	19.0	8.8	2.0	21.2	10.8	3.8		—			—			—			—	
		1 000	18.8	8.6	1.8	21.3	11.0	3.9		—			—			—			—	
11	2.0	1 100	19.5	10.6	1.8	21.0	11.8	3.4		—			—			—			—	
		1 000	19.5	10.2	1.6	21.3	12.0	3.5		—			—			—			—	
		900	19.7	10.1	1.5	22.3	12.4	3.6		—			—			—			—	
11	2.8	1 200	19.7	10.4	2.2	21.2	11.7	4.0		—			—			—			—	
		1 000	19.2	9.7	1.7	21.0	11.5	3.5		—			—			—			—	
		900	19.1	9.7	1.6	21.2	12.2	3.6		—			—			—			—	
11	3.0	1 200	19.0	10.2	2.4	20.7	11.7	4.1		—			—			—			—	
12	2.0	900		—			—		14.9	11.6	*	22.0	12.2	3.6		—			—	
12	2.8	1 200	19.1	11.9	2.2	20.4	12.8	3.8		—			—			—			—	
		1 100	19.0	11.1	1.8	20.7	12.3	3.3		—			—			—			—	
		1 000	18.9	10.8	1.7	20.6	12.3	3.3		—			—			—			—	
13	1.5	1 100		—			—		16.2	13.1	*	22.7	12.6	3.3		—			—	
		900		—			—		15.8	12.9	*	24.0	12.6	3.4		—			—	
13	2.0	1 100		—			—		14.8	12.9	*	21.2	12.6	3.3		—			—	
		900		—			—		14.3	12.8	*	21.7	12.9	3.6		—			—	
13	2.5	1 100		—			—		14.4	13.3	*	20.7	12.8	3.3		—			—	
16	2.5	1 200		—			—		15.9	18.5	*	20.8	15.7	3.0		—			—	

* Not determined

Table 2. Equilibrium composition of phases in Fe-30%Mn-Al-C alloys.

Composition of specimen (wt%)		Temp. (°C)	Compositions (wt%)																						
			$\gamma/\gamma+\kappa$			$\kappa/\gamma+\kappa$			$\alpha/\alpha+\kappa$			$\kappa/\alpha+\kappa$			$\gamma/\gamma+M_3C$			$M_3C/\gamma+M_3C$			$\alpha/\alpha+\gamma$			$\gamma/\alpha+\gamma$		
Al	C		Mn	Al	C	Mn	Al	C	Mn	Al	C	Mn	Al	C	Mn	Al	C	Mn	Al	C	Mn	Al	C	Mn	Al	C
3	2.8	1 100		—			—			—			—		29.7	3.3	2.9	39.0	0.2	7.4		—			—	
		1 000		—			—			—			—		26.7	3.5	2.4	40.3	0.2	7.3		—			—	
		900		—			—			—			—		25.0	3.9	2.2	41.4	0.3	7.3		—			—	
5	2.8	1 100	28.6	4.2	2.7	33.1	6.8	4.7		—			—			—			—			—			—	
		1 000	27.6	4.5	2.2	33.0	7.0	4.7		—			—			—			—			—			—	
		900	26.0	4.6	1.8	33.4	7.8	5.3		—			—			—			—			—			—	
7	3.0	1 100	27.4	6.1	2.4	31.2	8.1	4.8		—			—			—			—			—			—	
8	2.0	900	28.8	7.2	1.5	30.3	10.9	3.3		—			—			—			—			—			—	
8	2.5	1 200	30.1	8.1	2.4	32.7	9.6	4.6		—			—			—			—			—			—	
		1 100	28.5	7.5	2.4	31.9	9.3	4.4		—			—			—			—			—			—	
		1 000	28.1	7.4	1.8	31.9	9.4	4.4		—			—			—			—			—			—	
		900	26.2	6.5	2.0	32.7	9.2	4.1		—			—			—			—			—			—	
8	2.9	1 200	31.8	8.3	2.3	34.3	9.7	4.4		—			—			—			—			—			—	
		1 100	29.2	7.6	2.3	32.6	9.5	4.4		—			—			—			—			—			—	
		1 000	28.8	7.6	1.9	33.1	9.7	3.8		—			—			—			—			—			—	
		900	27.9	7.0	1.6	34.0	9.7	3.9		—			—			—			—			—			—	
9	2.4	1 200	30.2	9.2	2.3	33.4	10.4	4.3		—			—			—			—			—			—	
		1 000	27.8	8.2	1.7	31.6	10.2	4.2		—			—			—			—			—			—	
10	2.6	1 100	27.7	8.9	2.4	30.6	10.5	4.6		—			—			—			—			—			—	
10	3.0	1 200	29.3	9.8	2.1	31.4	10.9	4.0		—			—			—			—			—			—	
		1 100	27.2	8.8	2.1	30.0	10.5	4.1		—			—			—			—			—			—	
		900	25.7	8.4	1.7	30.1	10.6	4.0		—			—			—			—			—			—	
11	2.2	1 100	27.9	10.2	1.9	30.3	11.4	3.8		—			—			—			—			—			—	
		1 000	27.8	10.2	1.5	30.6	11.5	3.5		—			—			—			—			—			—	
12	0.5	1 100		—			—			—			—			—			—		26.5	12.4	*	30.6	10.9	1.3
		1 000		—			—			—			—			—			—		24.4	12.2	*	29.5	10.4	1.4
12	1.9	1 000	28.1	11.5	1.3	30.0	12.5	3.2		—			—			—			—			—			—	
12	2.4	1 000	27.6	11.0	2.1	29.9	12.2	4.1		—			—			—			—			—			—	
13	1.8	1 200	29.7	12.7	2.8	31.5	12.9	4.0		—			—			—			—			—			—	
		1 100	28.7	12.5	1.4	30.5	12.7	3.2		—			—			—			—			—			—	
		900		—			—		22.5	13.2	*	32.5	12.4	3.5		—			—			—			—		
14	1.8	1 200	28.6	13.2	2.6	30.2	13.2	3.5		—			—			—			—			—			—	
		1 100	28.2	13.7	1.4	29.7	13.7	2.9		—			—			—			—			—			—	
		1 000		—			—		22.7	14.8	*	30.4	13.2	3.4		—			—			—			—		
14	2.2	900		—			—		21.4	15.1	*	32.7	9.2	4.5		—			—			—			—		

* Not determined

Al/C=3.5/1. The $\kappa/\gamma+\kappa$ phase boundaries for both the Fe–20Mn and Fe–30Mn base alloys are consistent and have a tendency to retrogression, which is similar to the $\gamma'/\gamma+\gamma'$ phase boundary in the Ni–Al system.[22] Since the perovskite structure is one of the highly ordered fcc phases, the phase equilibrium between γ and κ phases is regarded as a miscibility gap due to ordering in the fcc phase. This can be supported by the fact that the modulated structure was observed in specimens of decomposed γ phase.[23,24] The present results on phase relationship given in Figs. 2 to 5 would be useful for designing and understanding of the microstructure in Fe–Mn–Al–C alloys.

3.2. *Transmission Electron Microscopy*

TEM observations were made on Fe–30Mn–(8–11)Al–1.2C alloys annealed between 600 and 1 100°C. Fig. 6(a) shows a microstructure annealed at 1 000°C for 150 h and quenched into water. The modulated-like structure was obtained and a similar structure was also observed in the specimen quenched from 1 100°C. Fig. 6(b) shows the diffraction pattern, which reveals the extra spots between the fundamental reflections. Furthermore, the fundamental reflections exhibit a streaking in the [010] direction as shown by the arrow in Fig. 6(b) and the absence of streaks in the superlattice reflections is recognized. The length and direction of the streaks depend on the order of reflection. The dark field image taken from (010) superlattice reflection is shown in Fig. 6(c). Very fine domains are seen within the matrix. All specimens showing the modulated-like structure in the bright field image exhibit the same structure in the dark field image as shown in Fig. 6(c). On the basis of this and the streaks of the diffraction spots as shown in Fig. 6(b), it was concluded that the streaks arose from the elastic distortion of the matrix due to the coherent precipitation of the second phase. Fig. 7(a) shows an electron micrograph of a specimen with the $\gamma+\kappa$ two-phase structure obtained by annealing at 900°C for 240 h. The diffraction patterns for the matrix γ and κ phases are shown in Figs. 7(b) and

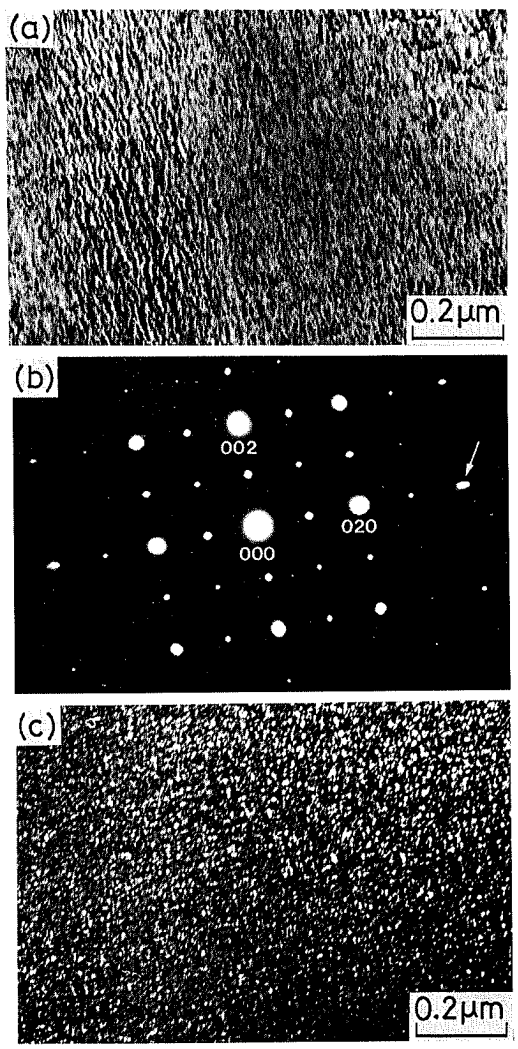

(a) Bright field micrograph
(b) Diffraction pattern having a [100] zone
(c) Dark field micrograph from (010) superlattice reflection

Fig. 6. Electron micrographs and diffraction pattern for Fe–30Mn–10.5Al–1.2C alloy quenched from 1 000°C.

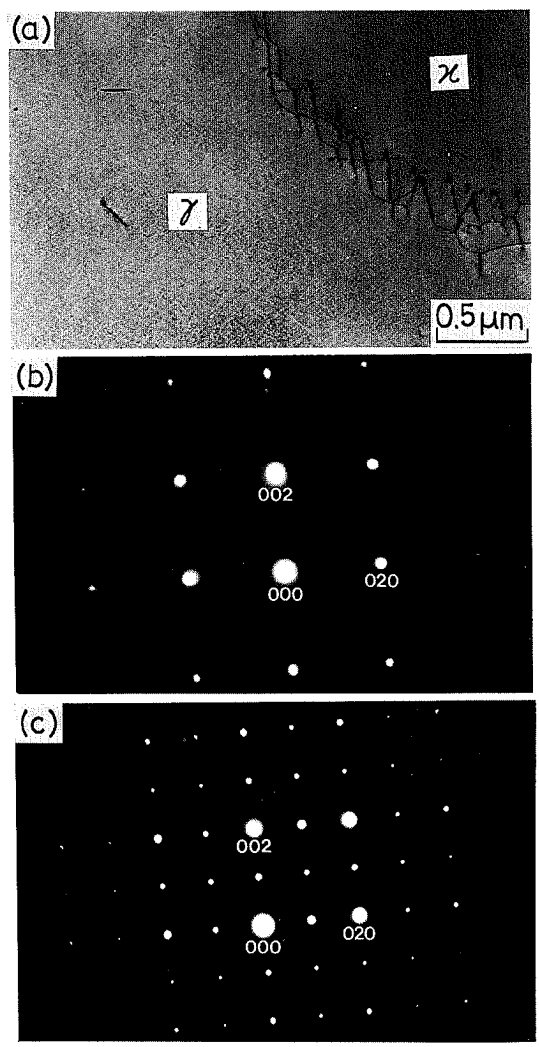

(a) Bright field micrograph
(b) Diffraction pattern taken from matrix
(c) Diffraction pattern taken from κ phase

Fig. 7. Electron micrograph and diffraction patterns for Fe–30Mn–11Al–1.2C alloy quenched from 900°C.

7(c), respectively. The misfit dislocations are observed at the interphase boundary between the γ and κ phases. The intensity of superlattice reflection from the matrix in Fig. 7(b) is very weak in comparison with that in Fig. 6(b). The electron micrograph of Fe–30Mn–8Al–1.2C alloy quenched from 800°C is shown in Fig. 8(a), where the rectangular features are identified as the κ phase according to the electron diffraction pattern. The moiré fringe is visible between the matrix γ and κ phases. Fig. 8(b) is the diffraction pattern from the matrix, where the superlattice extra reflections are not observed. The diffraction patterns for specimens quenched from 700 and 600°C also revealed that the matrix phase is of disorded structure. The superlattice reflections were observed only for the specimens quenched from the temperatures above 900°C. Since the diffraction patterns for the γ' phase with the $L1_2$ structure and the perovskite κ phase are very similar, it is necessary to carefully compare the intensities of diffraction spots from each phase. The structure factor for the γ' phase with randomly distributed carbon atoms is simply given by $F_{hkl}=f_{Al}-f_{Fe/Mn}$, where f_{Al} is the atomic scattering amplitude for Al atoms and $f_{Fe/Mn}$ is that for Fe or Mn atoms corrected according to their fraction. On the other hand, the structure factor for the κ phase can be written as

$$\begin{aligned} F_{hkl} &= \sum_n f_n \exp 2\pi i(hx_n+ky_n+lz_n) \\ &= f_{Al}+f_{Fe/Mn}\left[\exp 2\pi i\left(\frac{1}{2}h+\frac{1}{2}k\right)\right. \\ &\quad \left.+\exp 2\pi i\left(\frac{1}{2}k+\frac{1}{2}l\right)+\exp 2\pi i\left(\frac{1}{2}h+\frac{1}{2}l\right)\right] \\ &\quad +f_C \exp 2\pi i\left(\frac{1}{2}h+\frac{1}{2}k+\frac{1}{2}l\right) \end{aligned}$$

Since the numerical order of these atomic scattering amplitudes are $f_{Fe/Mn}>f_{Al}>f_C$, $|F_{hkl}|$ is more intense in the case where $h+k+l$ is odd than when $h+k+l$ is even. Taking the carbon content of the κ phase given in Table 2 into account, the structure factors for (100) and (110) reflections are calculated as listed in Table 3. The actual intensity of (100) spot for the κ phase is also much stronger than that of (110) reflection as shown in Fig. 7(c), being in good agreement with the expected intensity ratio. This fact supports that the phase in equilibrium with γ matrix shown in Figs. 1, 6(a), 7(a) and 8(a) is κ carbide. The observed superlattice reflections such as Fig. 6(b) also show that the intensity of (100) reflection is much stronger than that of (110) spot. All these results support the conclusion that the observed extra reflections are due to the presence of the κ phase rather than γ' phase, and are consistent with the observations on the rapidly solidified Fe–Mn–Al–C alloys.[8,9,14] Moreover, the specimens quenched from the single phase region of austenite at 1 000 and 1 100°C exhibit ferromagnetic. This fact also supports the precipitation of ferromagnetic κ phase during cooling. Therefore, it is concluded that the superlattice reflections taken from the specimens quenched from the temperatures above 900°C are from the precipitation of the κ phase during cooling.

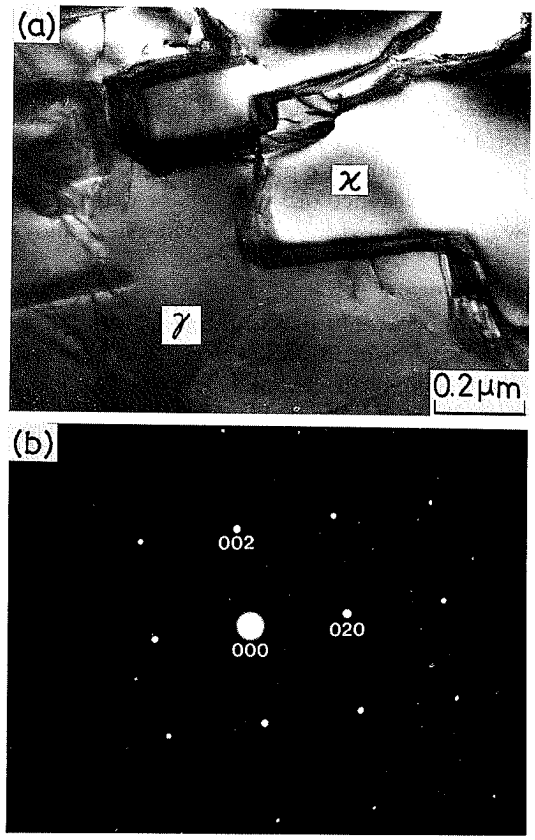

(a) Bright field micrograph
(b) Diffraction pattern taken from matrix

Fig. 8. Electron micrograph and diffraction pattern for Fe–30Mn–8Al–1.2C quenched from 800°C.

Table 3. Calculated structure factors for (100) and (110) superlattice reflections from γ' and κ phases.

	$\lvert F_{100}\rvert$	$\lvert F_{110}\rvert$	$\frac{\lvert F_{100}\rvert^2}{\lvert F_{110}\rvert^2}$
γ'	1.26	1.25	1.02
κ	3.13	0.35	81.7

4. Conclusion

The phase constitutions of Fe–(20–30)Mn–Al–C alloys were studied by EPMA and TEM. The results obtained were as follows.

(1) The phase relationships among α, γ and κ phases were established between 900 and 1 200°C. The κ phase with perovskite structure was formed in the high Al and high C regions.

(2) The stable region of austenite in Fe–30Mn–Al–C alloys was more extended than that in Fe–20Mn–Al–C alloys.

(3) The $\kappa/\gamma+\kappa$ phase boundaries exhibit a retrograde shape.

(4) A modulated-like structure was seen in Fe–30Mn–(8–11)Al–1.2C alloys quenched from 1 000 and 1 100°C.

(5) Superlattice reflections were observed in specimens quenched from the temperatures above 900°C, while no extra spots were confirmed for quenching after annealing at 800, 700 and 600°C.

(6) The observed superlattice reflections were due to the precipitation of κ phase during cooling.

(7) The existence of the γ' phase with $L1_2$ structure was not verified in bulk Fe–Mn–Al–C alloys.

Acknowledgments

The authors would like to thank Messrs. A. Satoh, now at Mitsubishi Metal Corp., and Y. Honma, Graduate School of Tohoku University, for their assistance in carrying out this work.

REFERENCES

1) S. K. Banerji: *Met. Prog.*, **113** (1978), No. 4, 59.
2) C. J. Altstetter, A. P. Bentley, J. W. Fourie and A. N. Kirkbride: *Mater. Sci. Eng.*, **82** (1986), 13.
3) J. Charles, A. Berghezan, A. Lutts and P. L. Dancoisne: *Met. Prog.*, **119** (1981), No. 5, 71.
4) Y. G. Kim, Y. S. Park and J. K. Han: *Metall. Trans. A*, **16A** (1985), 1689.
5) Y. G. Kim, J. K. Han and E. W. Lee: *Metall. Trans. A*, **17A** (1986), 2097.
6) J. E. Krzanowski: *Metall. Trans. A*, **19A** (1988), 1873.
7) J. Briggs, G. J. Russell and A. G. Clegg: *J. Mater. Sci.*, **18** (1985), 668.
8) A. Inoue, Y. Kojima, T. Minemura and T. Masumoto: *Trans. Jpn. Inst. Met.*, **20** (1979), 468.
9) A. Inoue, Y. Kojima, T. Minemura and T. Masumoto: *Metall. Trans. A*, **12A** (1981), 1245.
10) Z. Nishiyama, K. Shimizu and M. Harada: *J. Jpn. Inst. Met.*, **33** (1969), 871.
11) T. Tadaki, K. Shimizu and T. Watanabe: *Trans. Jpn. Inst. Met.*, **12** (1971), 386.
12) A. Inoue, T. Minemura, A. Kitamura and T. Masumoto: *Metall. Trans. A*, **12A** (1981), 1041.
13) S. A. Myers and C. C. Koch: *J. Mater. Res.*, **4** (1989), 44.
14) A. P. Bentley: *J. Mater. Sci. Lett.*, **5** (1986), 907.
15) M. Watanabe and C. M. Wayman: *Metall. Trans.*, **3** (1972), 2221.
16) R. Ohshima and C. M. Wayman: *Trans. Jpn. Inst. Met.*, **16** (1975), 111.
17) W. K. Choo and D. G. Kim: *Metall. Trans. A*, **18A** (1987), 759.
18) H. T. Chen, S. A. Myers and C. C. Koch: *Mater. Sci. Eng.*, **98** (1988), 277.
19) K. H. Han and W. K. Choo: *Metall. Trans. A*, **14A** (1983), 973.
20) Z. Sun, H. A. Davies and J. A. Whiteman: *Met. Sci.*, **18** (1984), 459.
21) W. K. Choo and K. H. Han: *Metall. Trans. A*, **16A** (1985), 5.
22) C. C. Jia, K. Ishida and T. Nishizawa: to be published in *Metall. Trans. A*.
23) K. Sato, K. Tagawa and Y. Inoue: *Scr. metall.*, **22** (1988), 899.
24) K. H. Han, W. K. Choo and D. E. Laughlin: *Scr. metall.*, **22** (1988), 1873.